ACS Catalysis

Research Article

pubs.acs.org/acscatalysis

Interference-Induced Broadband Absorption Enhancement for Plasmonic-Metal@Semiconductor Microsphere as Visible Light Photocatalyst

Song Sun, Huizhe Liu, Lin Wu, Ching E. Png, and Ping Bai*

Electronics and Photonics Department, Institute of High Performance Computing, Agency for Science, Technology and Research, 1 Fusionopolis Way, Singapore 138632, Singapore

Supporting Information

ABSTRACT: A fundamental study is performed on the surface plasmon resonance (SPR) of metal@semiconductor microsphere photocatalyst to uncover its broadband absorption mechanism over the visible wavelength region. Finite element method studies show that an interference pattern is uniquely generated inside the semiconductor microsphere due to the optical reflection and refraction at the interface between the microsphere and the catalytic medium. By embedding plasmonic nanoparticles (NPs) into the microsphere, an interference-induced broadband absorption enhancement over the entire visible region can be achieved as compared to other plasmonic structures. Based on the properties of the interference, the broadband absorption enhancement can be obtained everywhere inside the microsphere and is particularly large at the microsphere hot-zone. Studies also show that microsphere consisting of higher refractive index semiconductor can maximize the interference-induced broadband absorption enhancement. Besides, NPs with different materials can be mixed to tune the overall absorption band for flexible energy harvesting and enhanced selectivity. At the same time, the evanescent nature of the SPR near field could be better exploited to enhance the catalytic rate if locating the NPs close to the microsphere surface. Our findings could help experimentalists to design optimized metal@semiconductor microsphere photocatalyst to more efficiently utilize the solar power to drive chemical transformation.

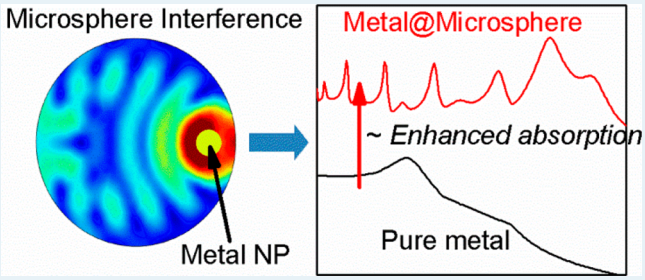

KEYWORDS: *photocatalysis, surface plasmon resonance, metals, semiconductors, microsphere, broadband absorption, interference*

1. INTRODUCTION

Photocatalysts absorb solar energy to drive the chemical reactions on the photocatalyst surface, which is considered to be an environmentally friendly approach to produce solar fuel or to remove pollutants. Metal oxide semiconductors are the most commonly used photocatalysts for a range of photochemical transformations, including H_2O splitting, CO oxidation, and dye degradation.[1−6] However, most metal oxide semiconductors possess large band gaps, which limit the light absorptions to high energy photon region (e.g., ultraviolet light) and exhibit a low conversion rate.[7,8] Although it is possible to extend the light absorption range using organic dye molecules or inorganic quantum dots,[9−12] they require energetically favorable band alignment and are rather unstable during the chemical reactions due to thermalized electron transfer.[10,13]

Other than dye molecules and quantum dots, plasmonic metal nanoparticles (NPs) have been recently demonstrated to extend light absorption over the visible wavelengths and significantly enhance the semiconductor catalytic rates due to the strong light−matter interaction at the metal surface called surface plasmon resonance (SPR).[14−18] It has been shown that SPR can enhance the catalytic rates based on two mechanisms. First, the SPR-excited nonthermalized electron at the metal surface possesses higher energy than the Schottky-barrier at the metal−semiconductor interface and thus can directly transfer to the semiconductor and induce photocatalytic transformation without requiring energetically favorable band alignment.[19−21] Second, the electron−hole generation rate in the semiconductor greatly increases due to the interaction of the semiconductor with the SPR-induced near field, which results in an enhancement in the photocatalytic rate.[22−24] Such a mechanism does not require intimate contact between metal and semiconductor and can transfer energy even if there is a gap or insulating medium between them.[14,25] In addition, the wavelength-dependent SPR enables flexible energy harvesting and can be potentially used to enhance the selectivity of catalytic transformation, which can never be achieved with conventional metal oxide semiconductor.[14,26,27]

Up to now, various plasmonic photocatalysts have been fabricated to realize the advantages of SPR, including metal sphere/cube,[28] metal−semiconductor composite,[15,16] metal-

Received: June 17, 2014
Revised: October 19, 2014
Published: October 20, 2014

loaded semiconductor film/fiber,[29] metal NP array,[30] and so forth. Among them, plasmonic metal NPs encapsulated by a large semiconductor microsphere (metal@semiconductor microsphere) particularly attracts our attention due to its enhanced photocatalytic rate,[18,31−33] large contact area,[33] easy storage, and good reusability.[18,34] For example, a high reduction rate of 4-nitrophenol has been achieved with the Fe_3O_4@SiO_2−Au microsphere (95% conversion in 12 min).[18] Despite the superior catalytic performance, the existing works are limited in developing the fabrication methods and simply attribute the enhanced catalytic rates to the extended SPR absorption in visible light region. No in-depth investigation has been performed to study the physical mechanism. In fact, the metal oxide semiconductor microsphere generally possesses high refractive index and large diameter size, which could significantly alter the electrical field distribution inside the microsphere and eventually lead to a different SPR broadband absorption compared to direct plasmonic-metal catalyst or small core−shell plasmonic catalyst. Nevertheless, the mechanism between the SPR broadband absorption and the microsphere field distribution is not yet clear. Furthermore, it is difficult to compare different plasmonic photocatalytic structures directly from the empirical measurements of catalytic rates as they depend not only on the plasmonic structures but also on other external conditions such as NP loading, temperature, pressure, among other factors. In contrast, the SPR broadband absorption depends only on the plasmonic structure, which indicates how much solar power can be exploited to drive the chemical reaction and is directly related to the ultimate catalytic rate. Therefore, studying the SPR broadband absorption allows us to compare different plasmonic structures, which guides the design and optimization of the catalyst.

The finite element method (FEM) is commonly adopted to analyze the plasmonic effect of metal NPs/nanostructures.[35] FEM is able to accurately compute not only the SPR absorption/scattering spectra but also the field distribution for either a single particle or a well-defined periodical structure,[36−38] regardless of its material compositions (e.g., can be pure metal or metal/semiconductor composite). With proper modification, our recent efforts have shown that even the quantum plasmon effect can be included in FEM simulation.[39,40] Nowadays, the study of SPR using FEM is widely accepted in many research fields such as sensing,[41] optical-modulator,[42] photocatalysis,[43] and the solar cell,[44] among others. These theoretical studies deepen the understanding of the mechanism of light−matter interaction and guide the design and optimization of the plasmonic structure. Due to its capability, we will use FEM throughout the paper.

In this contribution, we carry out a fundamental study on the SPR broadband absorption of metal@semiconductor microsphere using FEM by taking into account the interaction between the plasmonic NP and the field distribution inside the semiconductor microsphere. For the first time, we show that an interference field distribution pattern is generated inside the semiconductor microsphere due to the refractive index mismatch between the microsphere and the catalytic media. Consequently, the Au NP located at the constructive interference benefits from a field enhancement which eventually results in a broadband absorption enhancement over the entire visible region. Following that, we show that this interference-induced broadband absorption enhancement exists everywhere inside the microsphere and is particularly large at the microsphere hot-zone as compared to that of a direct plasmonic photocatalyst as well as small core−shell plasmonic photocatalyst. Such large broadband absorption enhancements enable the metal@semiconductor microsphere to better exploit the solar power to drive the chemical reaction, which could substantially enhance the photocatalytic rate. In the end, based on the properties of the microsphere interference, we also make a few suggestions for the experimentalists in designing the metal@semiconductor microsphere so as to optimize the photocatalyst performance.

2. THEORETICAL METHODS

2.1. Description of the Structure. The experimental metal@semiconductor microspheres usually contain multiple plasmonic metal NPs that complicate the physics by introducing plasmon-coupling events.[45] To simplify the problem, we focus on the most fundamental structure containing only one NP to better understand the physics. Figure 1 depicts the schematic of the studied structure, where a

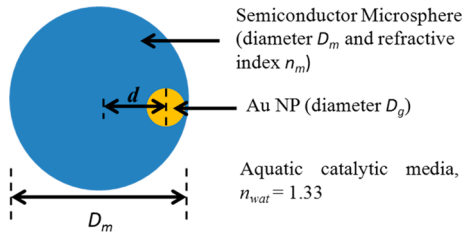

Figure 1. Schematic of plasmonic-metal@semiconductor microsphere.

plasmonic metal NP (diameter = D_g) is placed inside a semiconductor microsphere with diameter D_m and refractive index n_m. For illustrative purpose, Au NP is used, which typically exhibits a SPR in the visible light region (λ = 400−800 nm). Depending on the application, other plasmonic metal materials can be used (e.g., Ag, Cu, Al). Meanwhile, the semiconductor microsphere is assumed to be a homogeneous metal oxide (e.g., TiO_2) whose diameter D_m is comparable with or larger than the visible wavelength. However, more complex structures can also be implemented, such as a multilayer microsphere or hollowed microsphere.[18,33] Moreover, the Au NP is assumed to be completely encapsulated inside the semiconductor to prevent the NP from corrosion and dissolution,[18,46] where d is defined as the eccentricity between the center of the NP and the center of the microsphere. Nevertheless, the NP might also locate at the surface of the microsphere depending on the fabrication process.[32] In addition, the catalytic media outside the microsphere is assumed to be aqueous with n_{wat} = 1.33, whereas another medium might be applied depending on the catalytic environment. The dielectric constant of Au is taken from experimental measurement.[47]

2.2. Simulation with Finite Element Method. To study the SPR of the metal@semiconductor microsphere, it is essential to solve Maxwell's equations, whereby numerical or analytical techniques can be employed. The commonly used numerical approaches are boundary element method (BEM),[48] finite difference method (FDM),[49] and finite element method (FEM).[35] For the special case of spherical objects, the analytical method, Mie theory,[50] can be adopted. Mie theory is accurate and efficient; however, it is not applicable to nonconcentric spherical objects which are of important concern in our study.

dx.doi.org/10.1021/cs501399a | ACS Catal. 2014, 4, 4269−4276

BEM works better in surface problem rather than 3D volumetric geometry. Although FEM and FDM are both applicable for 3D geometry, FEM is more straightforward to handle the spherical geometry and has better approximation quality. Therefore, FEM will be exploited in this study with the commercial software COMSOL Multiphysics.

It is noteworthy that for small-sized plasmonic photocatalysts (D_m < 100 nm), we can calculate either the absorption cross-section (CS) or extinction CS to analyze its SPR.[15,28] However, due to the large diameter size of the metal@semiconductor microsphere, it is difficult to observe the SPR from the extinction CS which is dominated by the scattering field of the semiconductor microsphere. For example, Figure 2 proves this

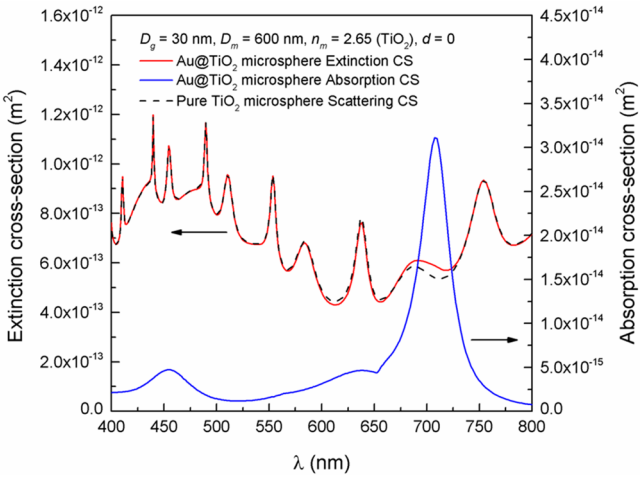

Figure 2. Comparison between the Au@TiO_2 microsphere and a pure TiO_2 microsphere at equal size. The absorption CS (blue solid curve) shows a much clearer SPR, whereas the extinction CS (red solid curve) of the Au@TiO_2 microsphere is dominated by the scattering CS of the pure TiO_2 microsphere (black dashed curve). The TiO_2 microsphere has diameter D_m = 0.6 μm and refractive index n_m = 2.65. The Au NP has diameter D_g = 100 nm and is located at the center of the microsphere (d = 0).

point by comparing the extinction CS of an Au@TiO_2 microsphere (red solid curve) and the scattering CS of an equal-size pure TiO_2 microsphere (black dashed curve). In contrast, the absorption CS can still demonstrate a clear SPR picture as it only results from the Au NP (blue solid curve). Therefore, it is more convenient to interpret the plasmon information from the absorption CS than the extinction CS. Hence, we focus on analyzing the absorption CS throughout the paper.

2.3. Verification of FEM Model. For verification purpose (Figure 3), we compared the absorption CSs from FEM and Mie theory for two previously reported plasmonic photocatalysts: (a) direct photocatalyst of an 30 nm Au NP directly contacting aqueous media without semiconductor shell (D_g = D_m = 30 nm, n_m = n_{wat} = 1.33),[14] (b) the small core–shell photocatalyst of an 30 nm Au NP uniformly coated with a 5 nm thick TiO_2 shell in aqueous media (D_g = 30 nm, D_m = 40 nm, n_m = 2.65, n_{wat} = 1.33).[17] The overall core–shell particle size is 40 nm, which is much smaller than the incident wavelength. The same plane wave excitations are used in FEM model and Mie theory for both cases. As expected, by coating the Au NP with higher refractive index semiconductor, the local permittivity surrounding the Au NP is increased, which leads

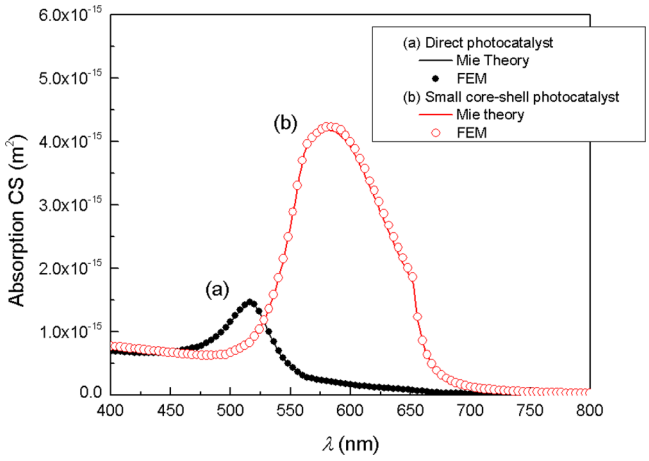

Figure 3. Verification of our FEM model using Mie theory for (a) direct photocatalysis of an 30 nm Au NP in water media (D_g = D_m = 30 nm, n_m = n_{wat} = 1.33) and (b) small core–shell photocatalysis of an 30 nm Au NP with 5 nm TiO_2 shell in water media (D_g = 30 nm, D_m = 40 nm, n_m = 2.65, n_{wat} = 1.33), which shows good agreement.

to a red-shift of the SPR wavelength. The results agree well, which show that our FEM simulations are reliable, and they will be used later as references to compare with the metal@semiconductor microsphere.

3. RESULTS AND DISCUSSION

3.1. Interference Field Distribution Pattern inside a Pure Microsphere. For the semiconductor microsphere whose diameter is comparable with or larger than the visible light wavelength, an interference field distribution pattern will be generated inside. The physical insight is briefly elaborated as follows (see n_m = 3 in Figure 4a): as the incident wave illumines on the microsphere, optical reflection and refraction will occur at the interface between A and B due to the refractive index mismatch between the microsphere and outside catalytic

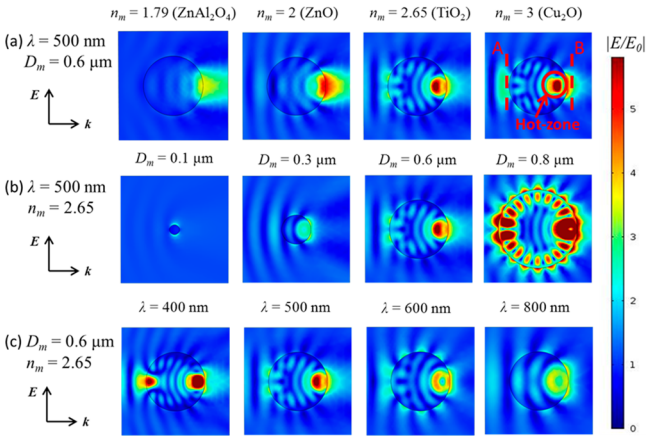

Figure 4. Normalized field distribution $|E/E_0|$ of a pure metal oxide semiconductor microsphere (no Au NP). An interference pattern inside the microsphere is more obvious at higher refractive index n_m, larger diameter D_m, and smaller wavelength λ. The bright region refers to a constructive interference, whereas the dark region refers to a destructive interference. From left to right, (a) n_m = 1.79, 2, 2.65, 3 at λ = 500 nm and D_m = 0.6 μm, (b) D_m = 0.1, 0.3, 0.6, 0.8 μm at λ = 500 nm and n_m = 2.65, (c) λ = 400, 500, 600, 800 nm at D_m = 0.6 μm and n_m = 2.65.

dx.doi.org/10.1021/cs501399a | ACS Catal. 2014, 4, 4269–4276

medium. The refracted wave at interface A will interact with the reflected wave at interface B, which eventually results in an interference pattern inside the microsphere. In our simulation, plane wave excitation is used to represent the large area illumination of the sunlight, whereby the light source is far away from the microsphere. The $E-k$ diagram in Figure 4 describes a plane wave with a wave vector k propagating rightwards and an electrical field polarization E pointing upward. Because the microsphere has a 3D symmetrical geometry, the resultant interference pattern is independent of the incident direction or the polarization. We will use this light incidence throughout the paper.

Figure 4a demonstrates the interference patterns for four metal oxide semiconductors that are used as photocatalysts, from left to right, n_m = 1.79 ($ZnAl_2O_4$), 2 (ZnO), 2.65 (TiO_2), and 3 (Cu_2O). It is clear that the interference becomes stronger at lager n_m as the amount of the reflected-wave at interface B increases on the basis of the Fresnel law.[51] The bright region refers to a constructive interference with larger electrical field enhancement $|E/E_0|$, whereas the dark region refers to a destructive interference with less or no enhancement. Particularly near interface B, a forward scattering effect is presented due to the spherical geometry of the semiconductor microsphere,[52] which forms a "hot-zone" with strongest field enhancement. Note that in principle, the interference pattern and the "hot zone" depend on the orientation of the photocatalyst with respect to the incident light direction. However, in our case, the microsphere has a 3D spherical symmetry, and thus, the orientation of the microsphere will not affect the interference pattern. The "hot zone" will appear at the opposite side of the microsphere with respect to the incident light direction (see Figure 4).

In addition, Figure 4b,c demonstrate the change of the interference pattern with respect to the microsphere diameter D_m and incident wavelength λ, which indicate that the interference becomes more prominent at larger D_m and smaller λ. The results can be understood with a wave theory: at constant incident wavelength λ, larger microsphere diameter D_m creates larger space for the reflected and refracted wave to interact. As a result, more wave periods can be established inside the microsphere (e.g., see D_m = 0.3 μm and D_m = 0.6 μm in Figure 4b). Similarly, at constant D_m, smaller λ equivalently increases the interaction space for the reflected and refracted wave and hence increases the numbers of wave periods inside the microsphere (e.g., see λ = 400 nm and λ = 800 nm in Figure 4c). A schematic illustration is presented in Figure S1 in the Supporting Information. It is noteworthy that the interference pattern becomes negligible at small diameter D_m < 0.1 μm. Hence, the small core–shell plasmonic photocatalyst (e.g., Figure 3b) does not have any interference effect.[17]

3.2. Interference-Induced Broadband Absorption Enhancement. The field enhancement $|E/E_0|$ introduced in the constructive interference region provides a convenient approach to evaluate the absorption enhancement of the Au NP. To demonstrate the effect, we first compare the absorptions of an Au NP at different locations inside the microsphere at incident wavelength λ = 500 nm. Figure 5a shows the interference field distribution $|E/E_0|$ inside the microsphere before adding the Au NP, where the semiconductor microsphere has D_m = 0.6 μm and n_m = 2.65, mimicking the properties of TiO_2. Inside the microsphere, 13 locations (from left to right, labeled as A–H) are selected to hold the Au NP (D_g = 30 nm), which are distributed with equal

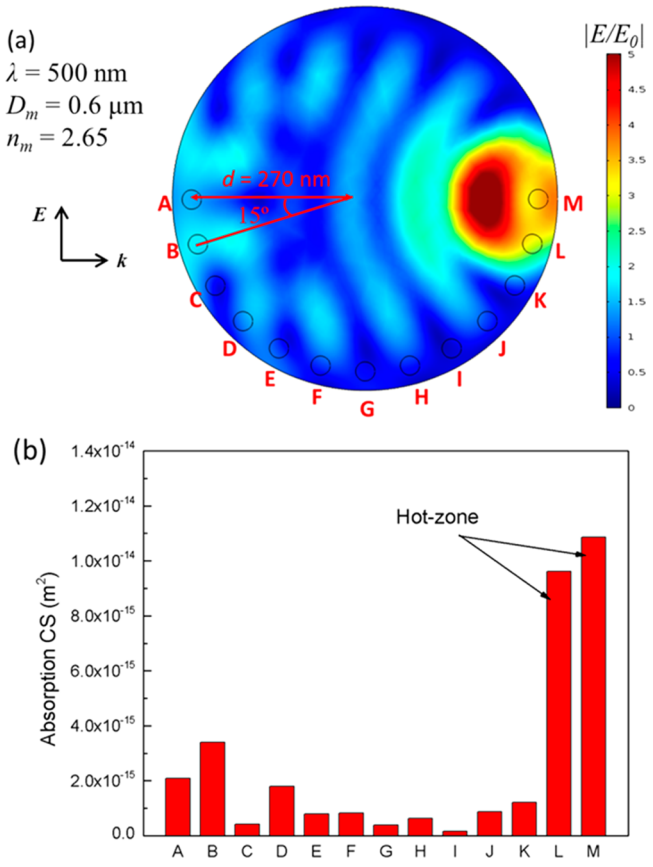

Figure 5. (a) Normalized field distribution $|E/E_0|$ inside the semiconductor microsphere (D_m = 0.6 μm and n_m = 2.65) at λ = 500 nm before adding the Au NP. Thirteen locations are selected to hold the Au NP, where A, B, D, L, M represent the constructive interference locations. (b) The absorption CS of an Au NP (D_g = 30 nm) at these locations. The absorption magnitudes are much greater for the NPs at the constructive interference region (A, B, D, L, M) than that in the destructive interference region.

eccentricity d = 270 nm and separated by a constant polar angle = 15°. Such structure mimics the real experimental metal@semiconductor microsphere that can be easily fabricated with the method introduced in the reference.[18] Note that A, B, D, L, M are located in the constructive interference with stronger field enhancement $|E/E_0|$, whereas the rest are located in the destructive interference with relatively weak field enhancement.

The resultant absorption CSs are shown in Figure 5b. As expected, the Au NPs located in the constructive interference region (A, B, D, L, M) possess larger absorption magnitudes than those in the destructive interference region, which is consistent with the interference field enhancement pattern in Figure 5a. In short, the Au NP at the constructive interference will benefit from a field enhancement that eventually results in an absorption enhancement. Because the interference pattern is generated due to the refractive index mismatch between the microsphere and the catalytic media, such absorption enhancement is a fundamental phenomenon that always exists regardless of the metal NP size or material.

Next, we proceed to examine the SPR broadband absorption over the visible light region (λ = 400–800 nm), which occupies 42–43% of the total solar energy on the earth surface. In this region, all the optical absorption comes from the SPR effect of the Au NP. Meanwhile, the TiO_2 microsphere can only absorb ultraviolet light (λ = 250–400 nm, occupying only 3–5% of the

dx.doi.org/10.1021/cs501399a | ACS Catal. 2014, 4, 4269–4276

total solar energy) with photon energy higher than the energy gap (~3.2 eV). Detailed absorption spectra of TiO_2 microsphere can be found in Figure S2 in the Supporting Information. According to Figure 4c, the interference pattern changes with respect to the incident wavelength λ. Thus, at a specific location inside the microsphere, the constructive interference would occur several times throughout the visible spectrum. Therefore, a broadband absorption enhancement is speculated for the Au NP inside the microsphere. For instance, Figure 6 shows the calculated broadband absorptions of the Au

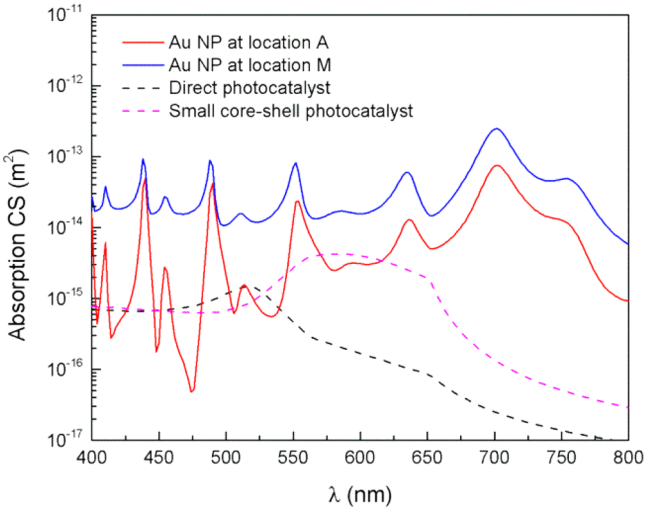

Figure 6. Broadband absorption over the visible spectrum for Au NP inside the microsphere at locations A (red solid curve) and M (blue solid curve), as well as direct photocatalyst (black dashed curve) and small core−shell photocatalyst (pink dashed curve). For Au NP at A and M, the absorption magnitudes are enhanced at multiple wavelengths due to the repeated occurrence of constructive interference throughout the visible spectrum, which eventually results in a broadband enhancement.

NPs at locations A (red solid curve) and M (blue solid curve). From the figure, multiple absorption peaks are observed, which indicate that the constructive interference arises repeatedly at different wavelengths. As a result, broadband absorption enhancements are achieved for the Au NP at both A and M as compared to that of direct photocatalyst (black dashed curve, same as Figure 3a) as well as small core−shell photocatalyst (pink dashed curve, same as Figure 3b).

Embedding the metal NP will alter the original interference pattern of the pure microsphere, because the resultant SPR is determined by the interaction of the metal NP and the interference pattern inside the semiconductor microsphere. However, this change only occurs locally, which is in the vicinity of the metal NP's surface. In terms of SPR physics, at the resonance condition, the collective oscillation of the electrons of metal NP will create a near-field wave in the *vicinity* of the metal NP.[53] This near-field wave is evanescent in nature, which decays exponentially away from the metal NP's surface.[54] Because the size of metal NP is generally much smaller than that of the semiconductor microsphere, the metal NP can only change the *local* interference pattern close to its surface and has no effect on other places. Detailed information can be found in Figure S3 in the Supporting Information.

To further strengthen our conclusion, we define a normalized absorption enhancement over the visible spectrum β_{ave} as an indicator for the broadband absorption enhancement. The expression of β_{ave} is shown in eq 1, where $Abs_M(\lambda)$ refers to the absorption of the Au NP (D_g = 30 nm) at various locations (A−M) inside the microsphere while $Abs_{ref}(\lambda)$ refers to the reference absorption which could be direct photocatalyst (Figure 3a) or small core−shell photocatalyst (Figure 3b). According to this definition, $\beta_{ave} > 1$ represents a broadband absorption enhancement, and the larger the β_{ave}, the larger the enhancement.

$$\beta_{ave} = \frac{\int_{400nm}^{800nm} Abs_M(\lambda)\cdot d\lambda}{\int_{400nm}^{800nm} Abs_{ref}(\lambda)\cdot d\lambda} \quad (1)$$

The results are recorded in Table 1 below, which show that there are broadband absorption enhancements ($\beta_{ave} > 1$) at all

Table 1. Normalized Absorption Enhancement β_{ave} at Different Locations (A−M) inside the Microsphere As Compared to Direct Photocatalyst and Small Core−Shell Photocatalyst[a]

locations in microsphere	β_{ave} compared to direct photocatalyst	β_{ave} compared to small core−shell photocatalyst
A	26.7	7.98
B	24.9	7.43
C	11.4	3.39
D	3.97	1.18
E	7.2	2.15
F	7.75	2.31
G	3.22	0.964
H	6.37	1.90
I	6.41	1.92
J	3.78	1.13
K	31.1	9.30
L (hot-zone)	82.2	24.6
M (hot-zone)	104	31

[a]The results imply a broadband absorption enhancement ($\beta_{ave} > 1$) at every location inside the microsphere.

studied locations (the only exception is position G compared to small core−shell photocatalyst β_{ave} = 0.964). These results can be extended to the remaining locations inside the microsphere as the interference occurs within the whole microsphere, which is particularly true when the microsphere is illuminated with the wide solar spectra. Especially for Au NP at the microsphere hot-zone (L and M), the broadband absorption can be enhanced more than 100 times than that of direct photocatalyst and 30 times than that small core−shell catalyst. For the real metal@semiconductor microsphere,[18,31−33] multiple Au NPs are distributed all over the microsphere, and there are always Au NPs locating at the hot-zone regardless of incident light direction and the microsphere orientation. Thus, the overall broadband absorption enhancement could be substantial. On the basis of this result, we conclude that the metal@semiconductor microsphere is a better catalyst structure in utilizing the solar power to drive the chemical reaction, which could subsequently lead to an enhanced photocatalytic rate.

3.3. Broadband Absorption Enhanced Direct Electron Transfer. In particular, the enhanced SPR broadband absorption presented in Table 1 can greatly enhance the capability of the Au@semiconductor microsphere to harvest the solar energy in the visible region, which directly improves the

dx.doi.org/10.1021/cs501399a | ACS Catal. 2014, 4, 4269−4276

photocatalytic rate through direct electron transfer mechanism (DET).[20,21,55−58]

Originally, it is believed that under the excitation of SPR, the conductive electrons at the metal NP surface will gain energy above its Fermi energy level, which is high enough to overcome the Schottky barrier created at the metal−semiconductor interface. As a result, these free electrons can move into the conduction band of the semiconductor and drive the chemical reaction.[20,21,55] Later, it is found that electron−hole pairs can be produced in the metal NP as the decay channels of the SPR. These hot electrons can then be directly injected into the semiconductor conduction band by a quantum tunneling process even with energy lower than the Schottky barrier.[56−58]

Based on the DET mechanism, the enhanced photocatalytic rate possesses the same spectral dependence as the SPR broadband absorption of metal NP.[16,21,57,59] Therefore, it is straightforward that the enhanced SPR broadband absorption of the Au@semiconductor microsphere will be translated into the enhancement of the photocatalytic rate.

Besides the DET, the SPR induced local electromagnetic field enhancement (LEMF) can also enhance the photocatalytic rate of Au@semiconductor microsphere by boosting the electron−hole generation rate at the semiconductor through interband transition.[22,23,28,60−62] Due to the nature of the interband transition, LEMF mainly boots the carrier generation beyond the semiconductor band gap energy, which is in the UV region.[16,22,23] In terms of this perspective, DET should be dominant in our case as the SPR enhance broadband absorption is mainly in the visible region.

3.4. Suggestions in Designing the Metal@Semiconductor Microsphere. On the basis of the properties of the microsphere interference, here we provide a few suggestions for the experimentalist in designing the metal@semiconductor microsphere in order to optimize the photocatalytic performance. First, because the interference becomes stronger as semiconductor refractive index n_m increases (see Figure 4), we recommend using higher refractive index semiconductor material to obtain larger broadband absorption. For instance, Figure 7 shows the broadband absorption for an Au NP at hot-zone M inside the microsphere with three different semiconductor materials: n_m = 1.79 ($ZnAl_2O_4$), n_m = 2 (ZnO), and n_m = 2.65 (TiO_2). Clearly, the Au NP possesses larger broadband absorption in the semiconductor with higher refractive index.

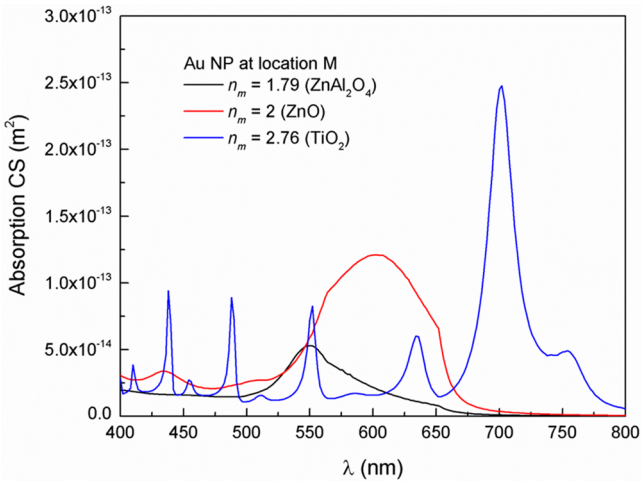

Figure 7. Broadband absorption for an Au NP at hot-zone M inside the microsphere with different semiconductor materials: n_m = 1.79 ($ZnAl_2O_4$), n_m = 2 (ZnO), and n_m = 2.65 (TiO_2). The Au NP has larger broadband absorption in semiconductor materials with larger refractive index.

Second, different plasmonic metal NPs can be mixed to adjust the overall absorption band of the metal@semiconductor microsphere, which would be useful in flexible energy harvesting and enhancing the selectivity.[14,26,27] Figure 8 shows the broadband absorptions of a 30 nm Au and Ag NP at hot-zone M, which exhibit different absorption bands. Recall that the interference pattern is a fundamental property of the semiconductor microsphere, and therefore, all the metal NPs inside can have broadband absorption enhancement regardless of the materials.

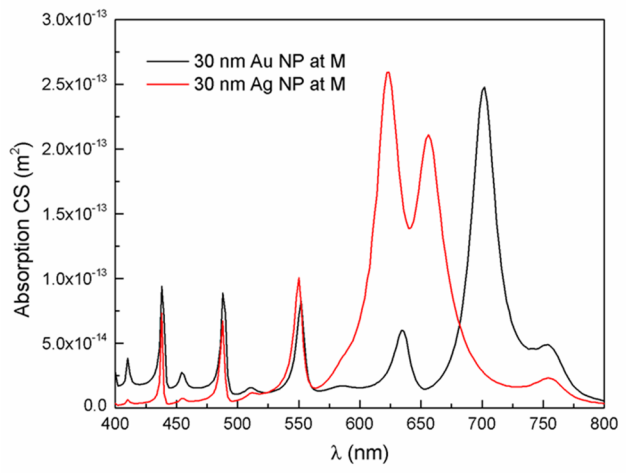

Figure 8. Broadband absorption for a 30 nm Au/Ag NP at the microsphere hot-zone M. Different metal NPs have different absorption bands, which can be mixed to adjust the overall absorption.

Lastly, we briefly discuss the effect of the eccentricity d, which is equivalent to the microsphere shell thickness in the experiment. Because the interference pattern exists within the entire microsphere, the broadband absorption enhancement should always exist regardless of the eccentricity d. For example, Table 2 records the normalized absorption enhancement β_{ave} at different eccentricity d, where the Au NP is originally located at A (d = 270 nm) and moving rightward toward the microsphere center (d = 0) at a 30 nm step. The result shows that the broadband absorption enhancement does exist ($\beta_{ave} > 1$) regardless of the eccentricity d. However, we do observe that the absorption enhancement is relatively larger near the surface of the microsphere (d = 270 or 240 nm). In addition, for photocatalysis application, it is recommended to control the NPs close to the surface of the semiconductor microsphere. This is because the plasmonic photocatalyst exploits SPR near field to improve the electron−hole generation in the semiconductor.[22−24] However, the SPR near field consists of evanescent wave that decreases exponentially with the distance away from the metal surface.[54] As a result, if the NPs are located too deep inside the microsphere, the charge generated at the vicinity of the NP surface will never reach the microsphere surface where the actual chemical transformation takes place. In contrast, if the NPs are close to the microsphere surface, their SPR near fields can channel the optical energy around the microsphere surface, hence improving the chemical

dx.doi.org/10.1021/cs501399a | ACS Catal. 2014, 4, 4269−4276

Table 2. Normalized Absorption Enhancement β_{ave} at Different Eccentricity d inside the Microsphere As Compared to Direct Photocatalyst and Small Core−Shell Photocatalyst[a]

eccentricity d [nm]	β_{ave} compared to direct photocatalyst	β_{ave} compared to small core−shell photocatalyst
270 (location A)	26.7	7.98
240	25	7.48
210	16.5	4.92
180	9.08	2.71
150	6.37	1.9
120	5.81	1.73
90	6.18	1.85
60	9.7	2.9
30	13.7	4.08
0 (center)	13.9	4.14

[a]The Au NP is originally located at A (d = 270 nm) and moving rightward towards the microsphere center (d = 0) at a 30 nm step. The broadband absorption enhancement (β_{ave} > 1) always exists regardless of d.

transformation efficiency.[63] In fact, this phenomenon has been observed in a previous experiment, in which the 4-nitrophenol reduction rate decreases as SiO_2 shell thickness increases.[18] Here we provide an explanation in terms of fundamental SPR physics. Note that if the Au NP is attached at the surface of the microsphere (e.g., d > 300 nm), there will be a blue-shift on the broadband absorption as compared to that of Au-inside microsphere due to the reduction on the local permittivity. Consequently, the broadband absorption effect of Au NP at the microsphere surface becomes less pronounced. The detailed information can be found in Figure S4 in the Supporting Information.

4. CONCLUSIONS

We have systematically studied the optical properties of the metal@semiconductor microsphere photocatalyst using finite element method. An interference pattern has been observed inside the semiconductor microsphere due to the refractive mismatch between the catalytic media and the semiconductor. The plasmonic NP located at the constructive interference experiences a field enhancement that results in a broadband absorption enhancement over the entire visible wavelength. This broadband enhancement exists everywhere inside the microsphere and is particularly large at the microsphere hot-zone near the surface of the microsphere. These results point out that metal@semiconductor microsphere can absorb more solar energy to drive the chemical reaction as compared to direct plasmonic photocatalyst or small core−shell plasmonic catalyst and hence could enhance the ultimate catalytic rate. On the basis of the properties of the microsphere interference, it is further suggested that higher refractive index semiconductor should be used to maximize the interference-induced broadband absorption, and different metal NPs can be mixed to tune the overall absorption band. Meanwhile, the NPs should be located close to the microsphere surface to maximize the catalytic rate due to the evanescent nature of the SPR near field. Our work provides not only a fundamental understanding of the SPR broadband absorption for metal@semiconductor microsphere but also guidance for the design of optimal plasmonic photocatalyst.

■ ASSOCIATED CONTENT

Supporting Information

The following files are available free of charge on the ACS Publications website at DOI: 10.1021/cs501399a.

Wave theory explanation, UV−vis absorption of a pure TiO_2 microsphere, SPR field distribution at different wavelengths, and SPR broadband absorption for eccentricity d = 270 − 315 nm (PDF).

■ AUTHOR INFORMATION

Corresponding Author

*E-mail: baiping@ihpc.a-star.edu.sg.

Notes

The authors declare no competing financial interest.

■ ACKNOWLEDGMENTS

The authors thank the Agency for Science, Technology and Research, Institute of Higher Performance Computing for support.

■ REFERENCES

(1) Kudo, A.; Miseki, Y. *Chem. Soc. Rev.* **2009**, *38*, 253−278.
(2) Wu, N. Q.; Wang, J.; Tafen, D. N.; Wang, H.; Zheng, J. G.; Lewis, J. P.; Liu, X.; Leonard, S. S.; Manivannan, A. *J. Am. Chem. Soc.* **2010**, *132*, 6679−6685.
(3) Li, J. T.; Meng, F. K.; Suri, S.; Ding, W. Q.; Huang, F. Q.; Wu, N. Q. *Chem. Commun.* **2012**, *48*, 8213−8215.
(4) Roy, S. C.; Varghese, O. K.; Paulose, M.; Grimes, C. A. *ACS Nano* **2010**, *4*, 1259−1278.
(5) Fujishima, A.; Zhang, X.; Tryk, D. A. *Surf. Sci. Rep.* **2008**, *63*, 515−582.
(6) Primo, A.; Corma, A.; Garcia, H. *Phys. Chem. Chem. Phys.* **2011**, *13*, 886−910.
(7) Meng, F. K.; Li, J. T.; Hong, Z. L.; Zhi, M. J.; Sakla, A.; Xiang, C. C.; Wu, N. Q. *Catal. Today* **2013**, *199*, 48−52.
(8) Kumar, M. K.; Krishnamoorthy, S.; Tan, L. K.; Chiam, S. Y.; Tripathy, S.; Gao, H. *ACS Catal.* **2011**, *1*, 300−308.
(9) Youngblood, W. J.; Lee, S. H. A.; Maeda, K.; Mallouk, T. E. *Acc. Chem. Res.* **2009**, *42*, 1966−1973.
(10) Ni, M.; Leung, M. K. H.; Leung, D. Y. C.; Sumathy, K. *Renewable and Sustainable Energy Rev.* **2007**, *11*, 401−425.
(11) Li, G.; Zhang, D.; Yu, J. C. *Environ. Sci. Technol.* **2009**, *43*, 7079−7085.
(12) Wang, D. F.; Zhao, H. G.; Wu, N. Q.; El Khakani, A.; Ma, D. L. *J. Phys. Chem. Lett.* **2010**, *1*, 1030−1035.
(13) Wang, B.; Kerr, L. L. *J. Solid State Electrochem.* **2012**, *16*, 1091−1097.
(14) Kale, M. J.; Avanesian, T.; Christopher, P. *ACS Catal.* **2014**, *4*, 116−128.
(15) Ingram, D. B.; Christopher, P.; Bauer, J.; Linic, S. *ACS Catal.* **2011**, *1*, 1441−1447.
(16) Li, J. T.; Cushing, S. K.; Bright, J.; Meng, F.; Senty, T. R.; Zheng, P.; Bristow, A. D.; Wu, N. Q. *ACS Catal.* **2013**, *3*, 47−51.
(17) Murdoch, M.; Waterhouse, G. I. N.; Nadeem, M. A.; Metson, J. B.; Keane, M. A.; Howe, R. F.; Llorca, J.; Idriss, H. *Nat. Chem.* **2011**, *3*, 489−492 DOI: 10.1038/nchem.1048.
(18) Deng, Y. H.; Cai, Y.; Sun, Z. K.; Liu, J.; Liu, C.; Wei, J.; Li, W.; Liu, C.; Wang, Y.; Zhao, D. Y. *J. Am. Chem. Soc.* **2010**, *132*, 8466−8473.
(19) Primo, A.; Corma, A.; Garcia, H. *Phys. Chem. Chem. Phys.* **2011**, *13*, 886−910.
(20) Tian, Y.; Tatsuma, T. *Chem. Commun.* **2004**, 1810−1811.
(21) Tian, Y.; Tatsuma, T. *J. Am. Chem. Soc.* **2005**, *127*, 7632−7637.
(22) Liu, Z. W.; Hou, W. B.; Pavaskar, P.; Aykol, M.; Cronin, S. B. *Nano Lett.* **2011**, *11*, 1111−1116.

(23) Hou, W.; Liu, Z.; Pavaskar, P.; Hung, W. H.; Cronin, S. B. *J. Catal.* **2011**, *277*, 149−153.
(24) Christopher, P.; Ingram, D. B.; Linic, S. *J. Phys. Chem. C* **2010**, *114*, 9173−9177.
(25) Cushing, S. K.; Li, J.; Meng, F.; Senty, T. R.; Suri, S.; Zhi, M.; Li, M.; Bristow, A. D.; Wu, N. Q. *J. Am. Chem. Soc.* **2012**, *134*, 15033−15041.
(26) Marimuthu, A.; Zhang, J.; Linic, S. *Science* **2013**, *339*, 1590−1593.
(27) Bonn, M.; Funk, S.; Hess, C.; Denzler, D. N.; Stampfl, C.; Scheffler, M.; Wolf, M.; Ertl, G. *Science* **1999**, *285*, 1042−1045.
(28) Linic, S.; Christopher, P.; Ingram, D. B. *Nat. Mater.* **2011**, *10*, 911−921.
(29) Liu, L. P.; Wang, G. M.; Li, Y.; Li, Y. D.; Zhang, J. Z. *Nano Res.* **2011**, *4*, 249−258.
(30) Pincella, F.; Isozaki, K.; Miki, K. *Light Sci. Appl.* **2014**, *3*, e133:1−6.
(31) Dong, F.; Li, Q. Y.; Zhou, Y.; Sun, Y. J.; Zhang, H. D.; Wu, Z. B. *Dalton Trans.* **2014**, *43*, 9468−9480.
(32) Wang, G. N.; Wang, X. F.; Liu, J. F.; Sun, X. M. *Chem.—Eur. J.* **2012**, *18*, 5361−5366.
(33) Kong, L. C.; Duan, G. T.; Zuo, G. M.; Cai, W. P.; Cheng, Z. X. *Mater. Chem. Phys.* **2010**, *123*, 421−426.
(34) Cho, E. C.; Choi, S. W.; Camargo, P. H. C.; Xia, Y. *Langmuir* **2010**, *26*, 10005−10012.
(35) Reddy, J. N.*An introduction to the finite element method*, 3rd ed.; McGraw-Hill: Singapore, 2005; pp 579−679.
(36) Zhao, J.; Pinchuk, A. O.; McMahon, J. M.; Li, S. Z.; Ausman, L. K.; Atkinson, A. L.; Schatz, G. C. *Acc. Chem. Res.* **2008**, *41*, 1710−1720.
(37) McMahon, J. M.; Henry, A. I.; Wustholz, K. L.; Natan, M. J.; Freeman, R. G.; Duyne, R. P. V.; Schatz, G. C. *Anal. Bioanal. Chem.* **2009**, *394*, 1819−1825.
(38) Chau, Y. F.; Jheng, C. Y. *Plasmonics* **2014**, *9*, 1−9.
(39) Tan, S. F.; Wu, L.; Yang, K. W.; Bai, P.; Bosman, M.; Nijhuis, C. A. *Science* **2014**, *343*, 1496−1499.
(40) Wu, L.; Duan, H. G.; Bai, P.; Bosman, M.; Yang, K. W.; Li, E. P. *ACS Nano* **2013**, *7*, 707−716.
(41) Hassani, A.; Skorobogatiy, M. *Opt. Express* **2006**, *14*, 11616−11621.
(42) Abedi, K.; Vahidi, H. *Front. Optoelectron.* **2013**, *6*, 290−296.
(43) Chen, J. J.; Wu, C. S.; Wu, P. C.; Tsai, D. P. *J. Phys. Chem. C* **2012**, *116*, 26535−26542.
(44) Brown, G. F.; Ager, J. W.; Walukiewicz, W.; Wu, J. *Sol. Energy Mater. Sol. Cells* **2010**, *94*, 478−483.
(45) Jain, P. K.; El-sayed, M. A. *Chem. Phys. Lett.* **2010**, *487*, 153−164.
(46) Wu, X. F.; Song, H. Y.; Yoon, J. M.; Yu, Y. T.; Chen, Y. F. *Langmuir* **2009**, *25*, 6438−6447.
(47) Palik, E. D. *Handbook of Optical Constants of Solid*; Academic Press: New York, 1985; Vol. *1*, pp 286−295.
(48) Wrobel, L. C.; Aliabadi, M. H. *The boundary element method*; John Wiley & Sons: New York, 2002; Vol. *2*, pp 491−517.
(49) Morton, K. W.; Mayers, D. F.*Numerical Solution of Partial Difference Equations: An Introduction*, 2nd ed.; Cambridge University Press: New York, 2005; pp 151−190.
(50) Liu, H. Z.; Mouthaan, K.; Zouhdi, S.; Leong, M. S. *Appl. Phys. A: Mater. Sci. Process.* **2012**, *109*, 189−196.
(51) Griffiths, D. J. *Introduction to Electrodynamics*, 3rd ed.; Prentice Hall: Upper Saddle River, NJ, 1999.
(52) Devilez, A.; Bonod, N.; Stout, B. *Proc. SPIE* **2010**, *7717*, 771708:1−9 DOI: 10.1117/12.855019.
(53) Li, E. P.; Chu, H. S.. *Plasmonic Nanoelectronics and Sensing*; Cambridge University Press: United Kingdom, 2014; pp 1−65.
(54) Marti, O.; Bielefeldt, H.; Hecht, B.; Herminghaus, S.; Leiderer, P.; Mlynek, J. *Opt. Commun.* **1993**, *96*, 225−228.
(55) Yu, J. G.; Dai, G. P.; Huang, B. B. *J. Phys. Chem. C* **2009**, *113*, 16394−16401.
(56) Furube, A.; Du, L.; Hara, K.; Katoh, R.; Tachiya, M. *J. Am. Chem. Soc.* **2007**, *129*, 14852−14853.
(57) Mubeen, S.; Hernandez-Sosa, G.; Moses, D.; Lee, J.; Moskovits, M. *Nano Lett.* **2011**, *11*, 5548−5552.
(58) Knight, M. W.; Sobhani, H.; Nordlander, P.; Halas, N. J. *Science* **2011**, *332*, 702−704.
(59) Subramanian, V.; Wolf, E. E.; Kamat, P. V. *J. Am. Chem. Soc.* **2004**, *126*, 4943−4950.
(60) Hou, W. B.; Cronin, S. B. *Adv. Funct. Mater.* **2013**, *23*, 1612−1619.
(61) Hou, W. B.; Hung, W. H.; Pavaskar, P.; Goeppert, A.; Aykol, M.; Cronin, S. B. *ACS Catal.* **2011**, *1*, 929−936.
(62) Lu, Y.; Yu, H. T.; Chen, S.; Quan, X.; Zhao, H. M. *Environ. Sci. Technol.* **2012**, *46*, 1724−1730.
(63) Michaels, A. M.; Brus, L. *J. Phys. Chem. B* **2000**, *104*, 11965−11971.